Global Journal of Researches in Engineering: A
Mechanical and Mechanics Engineering
Volume 19 Issue 3 Version 1.0 Year 2019
Type: Double Blind Peer Reviewed International Research Journal
Publisher: Global Journals
Online ISSN: 2249-4596 & Print ISSN: 0975-5861

Computational Fluid Dynamics and Experimental Analysis of a Coated Stainless Steel Gas Turbine Blade

By Leandro Augusto de Souza, Elisângela Martins Leal,
Adilson Rodrigues da Costa & Milton Sergio Ernandes d Lima
Federal University of Ouro Preto

Abstract- This Work Aims to Analyze, Through Computational Fluid Dynamics (Cfd)With the Concept of Conjugate Heat Transfer (Cht), the Effect of the Thermal Barrier Coating and the Cooling Systemon an Austenitic Stainless Steel Blade in Order to Evaluate the Temperature Behavior of the Material. Although this Steel Has a Lower Cost Compared Tto Super alloys, It has Similar Properties, Such as the Thermal Expansion Coefficient, Chemical Affinity and Melting Point. this Evaluation used Ansys® Cfx Software to Solve the Numerical Problem. the Systemis Validated by Comparing the Computational Results to an Experiment. Gas Turbine Blades have a Low Weight and an Elevated cost. this cost came Mainly from Both the Material used and the Sophisticated Coating and cooling Method. Thermal Barrier Coatings Associated to a Cooling System are Employed on Gas Turbine Blades to Increase the Lifetime of the Blade and the gas Turbine Performance.

Keywords: gas turbine; blade; computational fluid dynamics (CFD); stainless steel; conjugate heat transfer (CHT); thermal barrier coating (TBC).

GJRE-A Classification: For Code: 091405, 091499

Strictly as per the compliance and regulations of:

Computational Fluid Dynamics and Experimental Analysis of a Coated Stainless Steel Gas Turbine Blade

Leandro Augusto de Souza [α], Elisângela Martins Leal [σ] Adilson Rodrigues da Costa [ρ] & Milton Sergio Ernandes d Lima [ω]

Abstract- This work Aims to analyze, through computational fluid dynamics (Cfd) with the concept of conjugate heat transfer (Cht), the effect of the Thermal Barrier coating and the cooling systemon an Austenitic Stainless steel blade in order to Evaluate the Temperature Behavior of the Material. Although this Steel has a Lower cost compared to Super ALLOYS, it has Similar Properties, Such as the Thermal Expansion Coefficient, chemical Affinity and Melting point. this Evaluation used Ansys® Cfx Software ot Solve the Numerical Problem. the Systemis Validated by Comparing the computational Results to an Experiment. Gas Turbine Blades have a low weight and an Elevated cost. this cost came Mainly form both the Material used and the Sophisticated coating and cooling Method. Thermal Barrier Coatings Associated to a cooling System are Employed on gas Turbine Blades to Increase the Lifetime of the Blade and the gas Turbine Performance. the study Indicates that the Thermal Barrier coating and ahe cooling System were Efficient At Reducing the Temperature of the Metallic Substrate By 160°C. this can Indicated that Stainless steel Blades can be used in gas turbines where the Metallic Temperature limit was not be reached.

Keywords: gas turbine; blade; computational fluid dynamics (CFD); stainless steel; conjugate heat transfer (CHT); thermal barrier coating (TBC).

I. Introduction

Nowadays, gas turbines are used for power generation, mechanical drive, aircraft and marine propulsion [1-3]. In this sense, the gas turbine performance must be improved. Increase of 1% in turbine efficiency can mean millions of dollars in savings for the electric power producer, thus providing electricity to its customers at a lower cost [4].

From the thermodynamics viewpoint, the gas turbine performance can be improved mainly in two different ways, increasing both the turbine inlet temperature and the efficiency of the gas turbine components. The turbine inlet temperature is related to the blade material [5, 6] and the limiting factor has been associated with the working temperature of the blade material.

The increase in the turbine inlet temperature means the request of using super alloys associated with a sophisticated thermal barrier coating and advanced cooling methods. Many research centers are looking to develop new materials, new thermal barrier coatings and more efficient cooling systems in order to increase the efficiency of gas turbines [7]. Figure 1 shows the cooling system used in this research work for the experimental study.

In addition, the gas turbine blade operates in a harsh environment, where the components are subjected to corrosion and oxidation, centrifugal forces, high gas pressure, high gas velocity, high turbine inlet temperature and thermal and mechanical cycling, including fatigue and creep. All these issues are related to the most common failures in the turbine blades [8].

In this context, the thermal barrier coatings (TBCs) are used not only to increase the turbine inlet temperature but also to extend the turbine blade lifetime [9]. TBCs have a complex multilayer structure, which usually consists of four layers: top coat (TC), thermally grown oxide (TGO), bond coat (BC) and metallic substrate. TGO is formed between TC and BC due to reaction of oxygen and the aluminum present in BC [10]. Figure 1 shows this multilayer structure.

Author α ρ: Thematic Network in Materials Engineering, School of Mining, Federal University of OuroPreto, Minas Gerais, Brazil.
e-mails: adilson@em.ufop.br, lerler8@gmail.com
Author σ: Department of Mechanical Engineering, School of Mining, Federal University of OuroPreto, Minas Gerais, Brazil.
e-mail: elisangelamleal@ufop.edu.br
Author ω: Institute for AdvancedStudies-IEAv-DCTA, São José dos Campos, São Paulo, Brazil. e-mail: miltonsflima@gmail.com

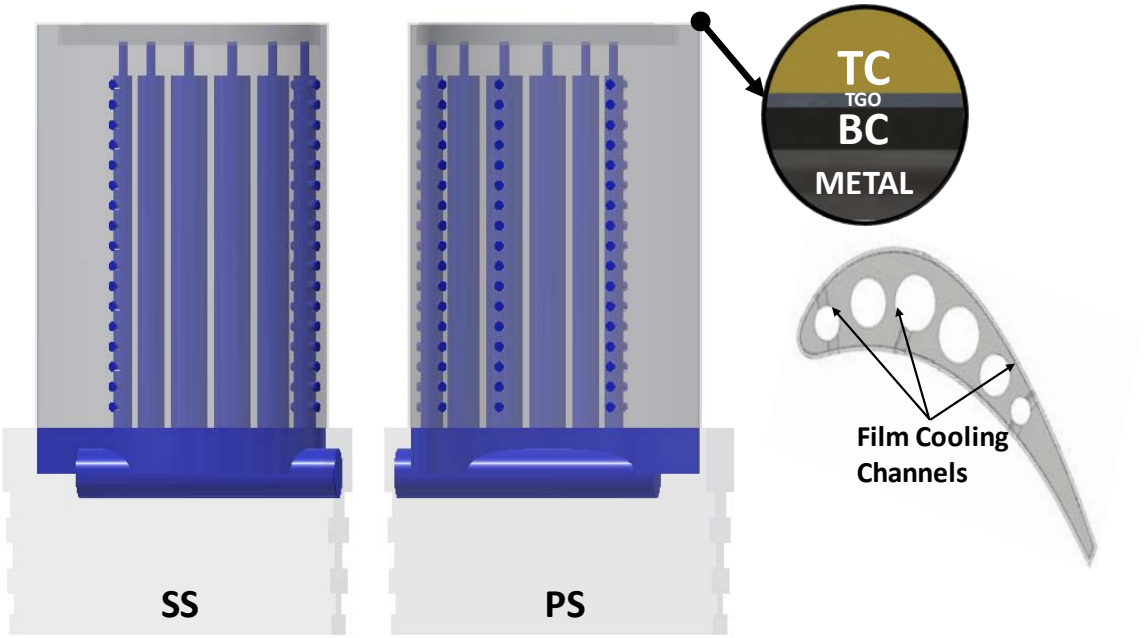

Figure 1: Blade Cooling System and Thermal Barrier Coating Layers.

The cooling system uses the compressor bypass air, which is at a relatively lower temperature than the gases from the combustion chamber. This air flows through the internal passages in the blade or through the skin and ejects into the hot gas mainstream to protect the blade surface from the hot mainstream gases. This process creates a thin film of the coolant fluid (called film cooling). Figure 1 also shows the coolant fluid path inside the blade [11].

Therefore, the metallic substrate is kept below the allowable temperature by using the cooling system and the thermal barrier coating [12]. In consideration of the commercial importance, the heat balance between the coated turbine blade, the cooling system, and a given intake temperature has been subject of many computational simulations.

The simulation of a turbine blade is a complex 3-D problem, which requires a multidisciplinary approach, including fluid dynamics and structural analysis. For example, in the cooled turbines, the blade temperature can be calculated simulating the internal coolant fluid, external hot gas and metal conduction simultaneously by the conjugate heat transfer (CHT) method. The CHT method produce a more accurate approximation to the convective heat transfer, and thus the temperature could be predicted more accurately. This problem can be solved by determining the flow of the fluid around the blade, the fluid-solid interaction and the turbine blade response to thermo-mechanical loading [13-15].

The restrict conditions for the static analysis occur when the parameters such as speed and temperature are in a steady state, the turbine is in full operation, and has a certain equilibrium, where there are no variations with time. However, from this analysis it is not possible to state its behavior at the start and the shutoff of the engine, or when there are variations in the time of some parameter [30].

Several researchers have applied the conjugate heat transfer on turbine systems. Bohn et al. [16,17] made conjugated calculation in a turbo machinery and investigate leading edge film cooling. Bohn et al. [18] shows that the conjugated calculation gives a more accurate temperature distribution and the predicted life span of the component is more plausible.

This work aims to analyze through computational fluid dynamics (CFD) with the concept of conjugate heat transfer (CHT), the effect of the thermal barrier coating of an austenitic stainless steel gas turbine blade. Although this steel has a lower cost compared to super alloys, it has similar properties, such as the thermal expansion coefficient, chemical affinity and melting point [19-21]. Thus, the stainless steel AISI 304 and AISI 316 can be used as a blade alternative substrate. An experiment has been performed where the turbine blade was placed in a furnace, simulating the gas turbine work environment in order to validate the results of the simulation.

II. Methodology

a) Materials

The metallic substrate used in this work consisted of the stainless steel AISI 316. The stainless steel blade was shaped by machining, and the final dimensions are shown in Figure 2. The TBC consisted of a layer of Ni Cr AlY as the bond coat and an yttria-stabilized zirconia (YSZ) as the top coat. All coatings were deposited using combustion thermal spraying.

b) Computational domain and numerical model

The shape of the rotor blade was based on a GT-100 gas turbine design [22]. The blade has six coolant passages, a constant cross section, to allow film cooling. The blade has 85 holes on the pressure and suction surfaces. The construction details are shown in Figure 3. In this paper, multiple layers were added over the metallic substrate, i.e. the bond coat NiCrAlY was added upon the metallic substrate and the top coat YSZ was added upon the NiCrAlY. The thicknesses of the BC and TC were 100 μm and 500 μm, respectively, in accordance with Clarke et al. [23].

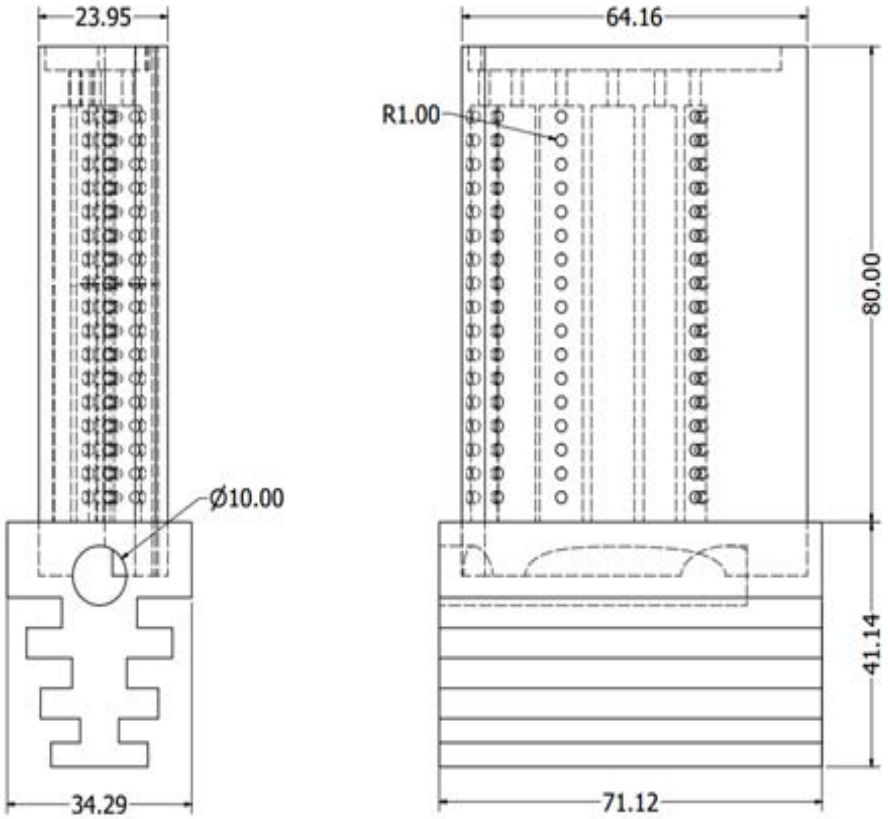

Figure 2: Blade main dimensions (mm).

Figure 3: Rotor blade with film cooling channels.

The section of the 3D computational multi-block grid mesh of the gas turbine blade is shown in Figure 4. This figure shows the elements of the solid domain, where the orange layer is the top coat, the green layer is the bond coat and the gray part is the stainless steel. The fluid domain is also shown in Fig. 4. The computational domain is comprised of the fluid regions around and inside the blade and the solid material domain of the TBC and the metallic substrate. Both tetrahedral and hexahedron cells are applied at the interface between the external fluid/YSZ and internal fluid/substrate. The grids of the interface between the solid domain and the fluid domain surface must be the same, and to improve the viscous boundary layer, the y+ was close to one [24].The total number of cells is 7,292,331, including 3,611,007 cells in the fluid domain and 3,681,304 cells in the solids domains (metallic substrate and the thermal barrier coating).

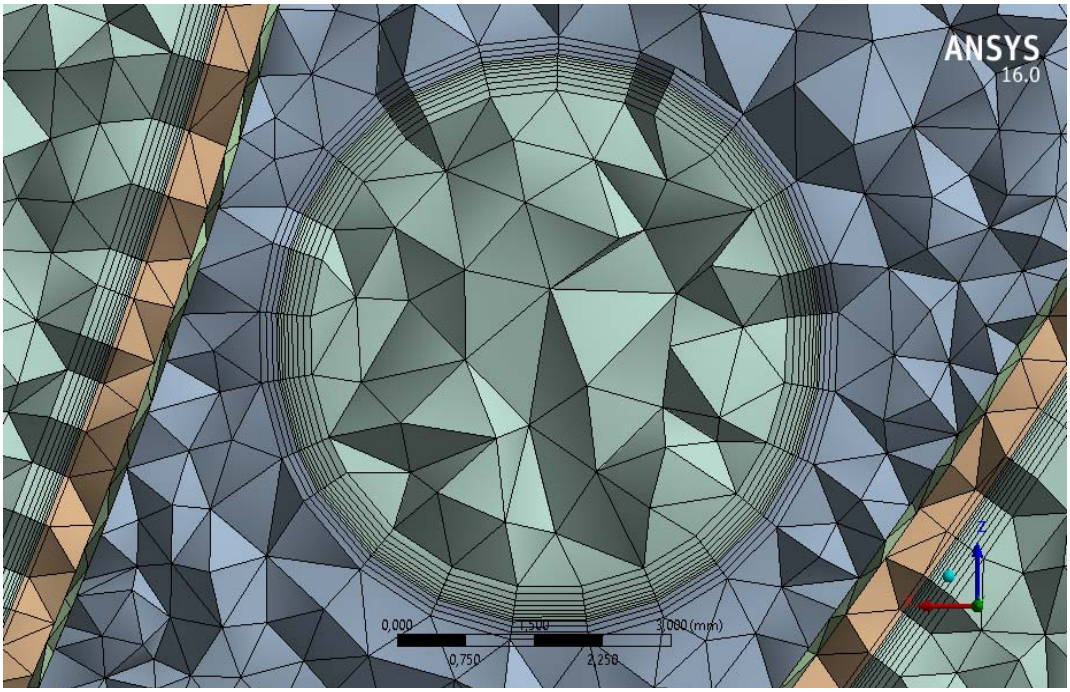

Figure 4: Representation of the 3D mesh section with the solid and fluid domain.

The numerical analyses were performed using the commercial software ANSYS CFX V.16.0, based on the finite volume method, and applying the CHT method. A steady-state analysis was fulfilled using shear stress transport turbulence model, also known as SST k-omega model, considering boundary transition and the perfect gas law was used as the equation of state [25].

c) Governing equations – CFD Problem

The governing equations for the computational fluid dynamics are based on Navier-Stokes equations. In this sense, three transport equations are used to solve the problem [26]. The mass conservation is:

$$\frac{\partial \rho}{\partial t} + \nabla(\rho\, U) = 0 \tag{1}$$

The momentum conservation is [26]:

$$\frac{\partial (\rho\, U)}{\partial t} + \nabla(\rho\, U \times U) = -\nabla p + \nabla \tau + S_M \tag{2}$$

In addition, the energy conservation is [26]:

$$\frac{\partial (\rho\, h_{tot})}{\partial t} - \frac{\partial p}{\partial t} + \nabla(\rho\, U\, h_{tot}) = \nabla(\lambda\, \nabla\, \mathrm{T}) + \nabla(\mathrm{U} \cdot \tau) + U \cdot S_M + S_E \tag{3}$$

The conjugate heat transfer analysis made a heat balance between the convection in fluids (external and internal fluid) and the conduction in solids. The convection and the conduction equations are [25]:

Convection:
$$\frac{\partial f}{\partial t} + V\nabla(f) = 0 \tag{4}$$

Conduction:
$$\frac{\partial T}{\partial t} = div(\alpha \nabla \mathrm{T}) \tag{5}$$

The conjugate heat transfer also uses the energy conservation equation (equation 3) for fluid and solid domains in the same matrix. Then, the interfaces between fluids and solids can be treated in an implicit way by discretizing the energy flux. Therefore, the continuity of the temperature distribution between every interface is respect at each iteration [25].

d) Boundary conditions – CFD Problem

The inlet mass flow for the external fluid was fixed as 0.5kg/s. The angular velocity of the blade was

3,600rpm. The inlet temperature of the coolant fluid was set at 127 ° C, the inlet mass flow of the coolant fluid was set as 4% of the inlet mass flow of the external fluid, i.e. 0.002kg/s. Four values were used for the turbine inlet temperature: 900°C, 1000°C, 1100°C and 1200°C. The inlet temperature profile was used to emulate a real combustor outlet profile, as known as, the Radial Temperature Distortion Factor (RTDF), as can be seen in Figure 5 [25].

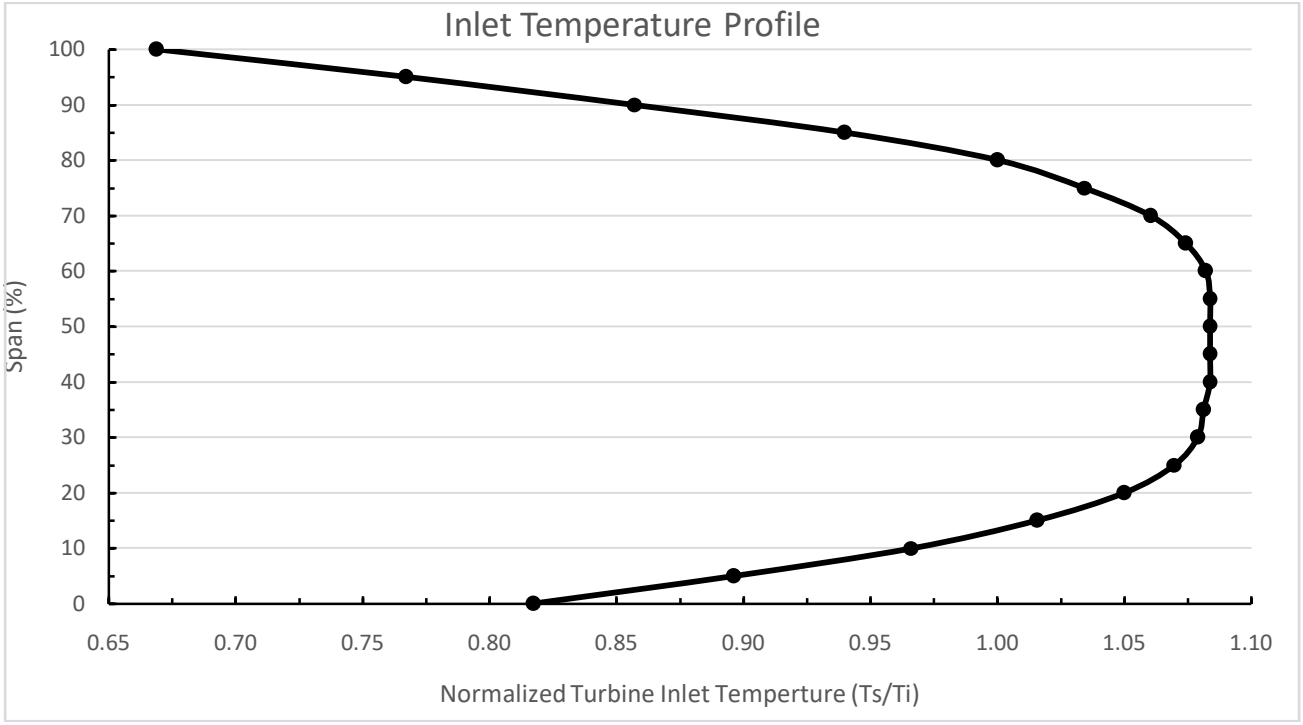

Figure 5: Turbine Inlet Temperature Profile.

The thickness of the bond coat and the top coat were set as100μm and 500μm. The interface between the solid layers is assumed to be perfect and without contact thermal resistance. Table 1shows the material thermal properties.

Table 1: Material Properties used for the Thermal Analysis [24,27]

Material	Temperature (°C)	Thermal Conductivity (W/m.K)	Specific Heat (J/kg.K)	Specific Mass (kg/m^3)	Thermal expansion coefficient (10^{-6}/°C)
Yttria-stabilized Zirconia	25-100	1.05	483	5,650	9.68
	400	--	--	--	--
	800	--	--	--	9.88
	1000	--	--	--	10.34
NiCrAlY	25-100	4.30	501	7,320	--
	400	6.40	592	--	12.50
	800	10.20	781	--	14.30
	1000	16.10	764	--	16.00
Stainless Steel AISI 316	25-100	16.3	500	8,000	17.5
	400	--	--	--	17.5
	800	--	--	--	--
	1000	--	--	--	--

The solver was performed to a single blade, and periodic conditions were applied to the lateral limitations of the fluid domain. Nevertheless, the results from this solver could be applied to several blades composing the rotor stage of the turbine.

e) Governing Equations – Static Structural Problem

For the static structural analysis, the governing equations are based on the equilibrium equations [26]:

$$\frac{\partial \sigma_x}{\partial x} + \frac{\partial \tau_{xy}}{\partial y} + \frac{\partial \tau_{xz}}{\partial z} + f_x = 0 \quad (6)$$

$$\frac{\partial \tau_{xy}}{\partial x} + \frac{\partial \sigma_y}{\partial y} + \frac{\partial \tau_{yz}}{\partial z} + f_y = 0 \quad (7)$$

$$\frac{\partial \tau_{xz}}{\partial x} + \frac{\partial \tau_{yz}}{\partial y} + \frac{\partial \sigma_z}{\partial z} + f_z = 0 \quad (8)$$

On the 3D-Hook's Law [26]:

$$\begin{bmatrix} \sigma_x \\ \sigma_y \\ \sigma_z \\ \tau_{yz} \\ \tau_{xz} \\ \tau_{xy} \end{bmatrix} = \frac{E}{(1+\nu)(1-2\nu)} \begin{bmatrix} 1-\nu & \nu & \nu & 0 & 0 & 0 \\ \nu & 1-\nu & \nu & 0 & 0 & 0 \\ \nu & \nu & 1-\nu & 0 & 0 & 0 \\ 0 & 0 & 0 & 1-2\nu & 0 & 0 \\ 0 & 0 & 0 & 0 & 1-2\nu & 0 \\ 0 & 0 & 0 & 0 & 0 & 1-2\nu \end{bmatrix} \begin{bmatrix} \varepsilon_x \\ \varepsilon_y \\ \varepsilon_z \\ \gamma_{yz} \\ \gamma_{xz} \\ \gamma_{xy} \end{bmatrix} \quad (9)$$

And on the strain-displacement relations [26]:

$$\varepsilon_x = \frac{\partial u}{\partial x} \quad (10)$$

$$\varepsilon_y = \frac{\partial v}{\partial y} \quad (11)$$

$$\varepsilon_z = \frac{\partial w}{\partial z} \quad (12)$$

$$\gamma_{xy} = \frac{\partial u}{\partial y} + \frac{\partial v}{\partial x} \quad (13)$$

$$\gamma_{yz} = \frac{\partial v}{\partial z} + \frac{\partial w}{\partial y} \quad (14)$$

$$\gamma_{zx} = \frac{\partial w}{\partial x} + \frac{\partial u}{\partial z} \quad (15)$$

The static structural analysis was supplied by

Therefore, there are 15 equations (from equation (6) to equation (15), equation (9) has six equations in a matrix form) and 15 unknowns, which must be evaluated.

f) Boundary Conditions – Static Structural Problem

The static structural analysis was supplied by the computational fluid dynamics solution. The forces created by the fluid will be the input parameters, and the material properties, as shown in Table 2, would be applied for each material.

Table 2: Material Properties for Structural Analysis [27-29]

Material	Temperature T (°C)	Elastic Modulus E (GPa)	Poisson Coefficient ν
Yttria-stabilized Zirconia (YSZ)	25 - 100	222	0.25
	400 - 1500	180	--
NiCrAlY	25 - 100	231 – 226.5	0.30
	800	117	--
Stainless Steel AISI 316	25 - 100	193	0.30
	--	--	--

The base of the blade was supposed to be rigid, since it is fixed to the disc, and it is imposed a given rotation of the shaft of 3600 rpm.

g) Experimental Procedure and validation of the numerical method

The experiments were performed in a furnace powered by combustion gases from LPG (Liquefied Petroleum Gas) firing. The burning was made by a blowtorch. In this set-up, the blowtorch was placed in a position that only the combustion gases pass through the blade. In order to keep the heat inside the furnace, the space between the blowtorch and the leading edge of the blade was covered by refractory bricks. A schematic draw of the furnace is show in Figure 6.

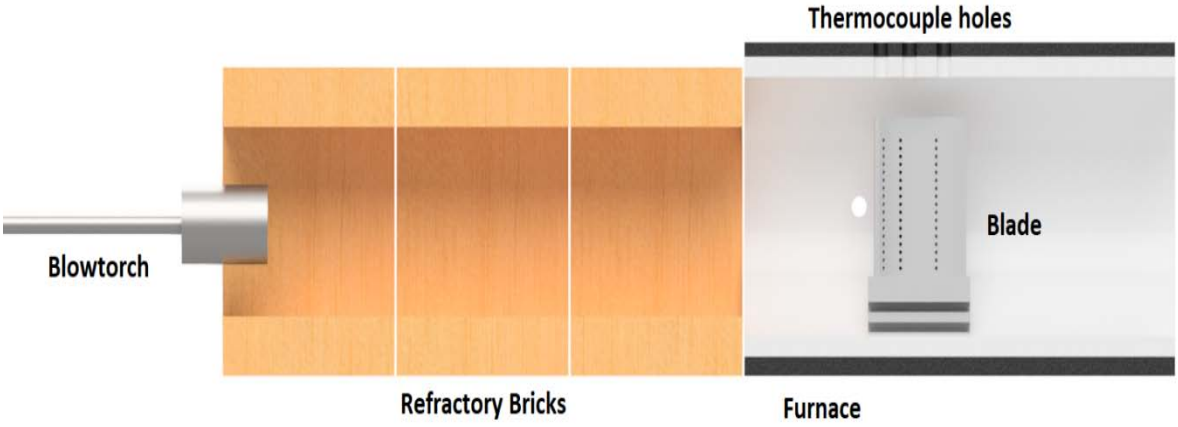

Figure 6: Schematic draw of the furnace.

The inlet temperature was measured by a thermocouple close to the leading edge of the blade. Moreover, the internal temperature was measured by three thermocouples that were inside in three cooling channels. One thermocouple was inside the channel close to the leading edge, another thermocouple was inside the channel close to the middle of the blade and another one into the channel close to the trailing edge. In order to record the temperature, the thermocouples were coupled to a Eurot herm 2132 system.

The validation of the simulation was based on the comparison between the values found in the experiment and in the simulation. Table 3 shows the errors between the simulation temperature and the experimental temperature at leading edge, intermediate region and the trailing edge.

Table 3: Errors for each turbine inlet temperature

Turbine Inlet Temperature (°C)	Error in Leading Edge (%)	Error in Blade Center (%)	Error in Trailing Edge (%)
900	6	8	9
1000	3	4	4
1100	7	5	3
1200	5	4	6

The simulation has a good fit to the experiment showing an adequate degree of accuracy with the reality predicted by the experiment. The maximum error occurred in the trailing edge at 900°C.

III. Results and Discussion

In the following paragraphs, the main aspects regarding the influence of each turbine inlet temperature on the stainless steel blade for the simulation and the furnace experimental will be evaluated.

a) Thermodynamics – Furnace

Table 4 shows the gas turbine blade internal temperatures of the wall close to the leading edge, to the blade center and to the trailing edge.

Table 4: Measured blade internal temperatures

Turbine Inlet Temperature (°C)	Temperature Leading Edge (°C)	Temperature Blade Center (°C)	Temperature in Trailing Edge (°C)
900	598	538	623
1000	687	601	701
1100	782	753	811
1200	875	816	884

The differences between the turbine inlet temperature and the measured temperatures are shown in Figure7.This figure shows that blade center has high temperature difference because the cooling system effect is high at the blade center.

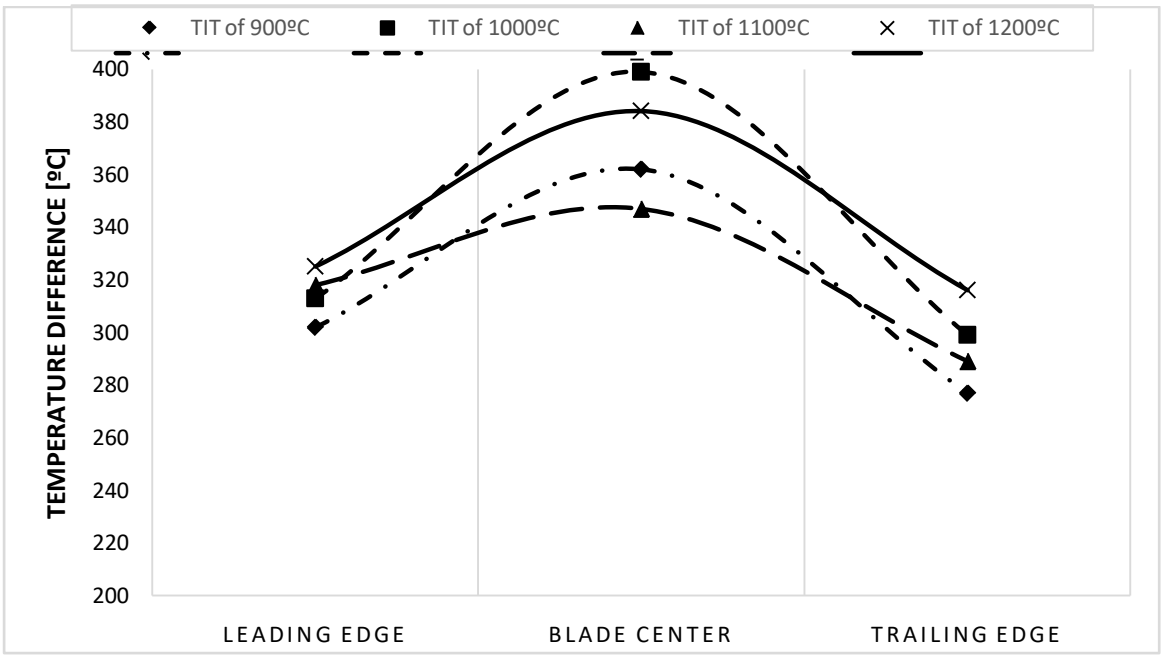

Figure 7: Temperature difference between the turbine inlet temperature (TIT) and the internal temperature

Figure 7 shows that the coating and the cooling system was able to reduce approximately 315°C on the cooling channels close to the leading edge, decrease approximately 373°C on the blade center and reduce 295°C on the trailing edge. Thus, the cooling system has great influence over the blade center and low significance over the trailing edge.

b) External Aerodynamics

The surface oil flow of each turbine inlet temperature are similar to each other. Then, the surface oil flow of the blade in the pressure and suction side, is shown in Fig.8. The stagnation line is close to the leading edge. Then, the flow is separated, part goes to the suction side and other part goes to pressure side, generated by the horseshoe vortex (green arrows) that appears next to the leading edge. The Figure 8 also shows tip leakage flow (blue arrows) starts from the tip region of the blade pressure side. At the tip region of the suction side, the cooling air triggers a secondary vortex that grows toward the mid-span of trailing edge because of the influence of the cooling air.

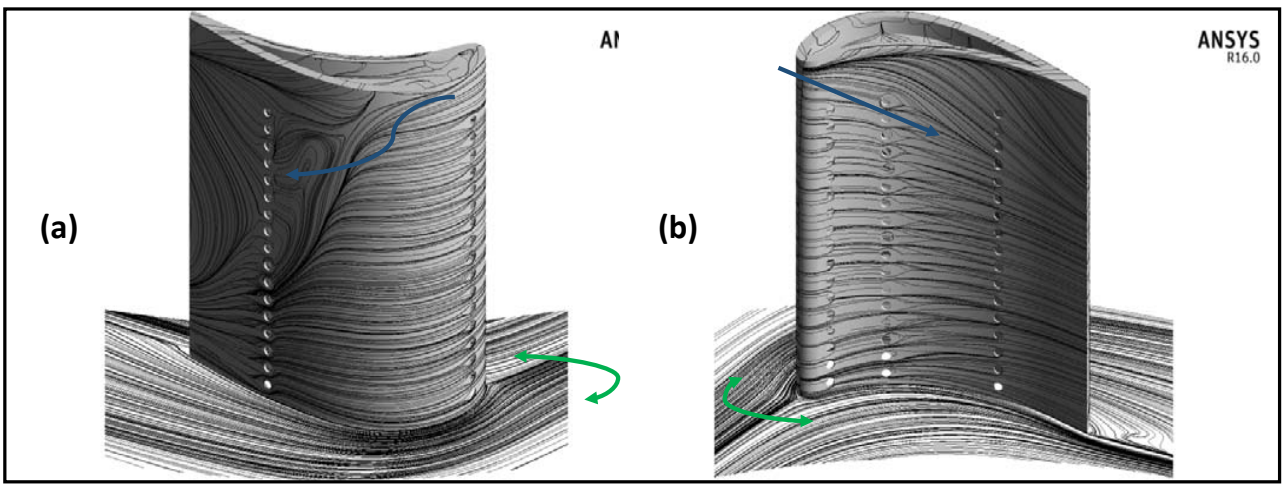

Figure 8: Surface oil flow (a) suction side and (b) pressure side.

The velocity distribution of the external and internal flow at a cross section of the blade at 50% of the height is shown in Figure9. This figure shows the velocity distribution for the four mentioned turbine inlet temperatures.

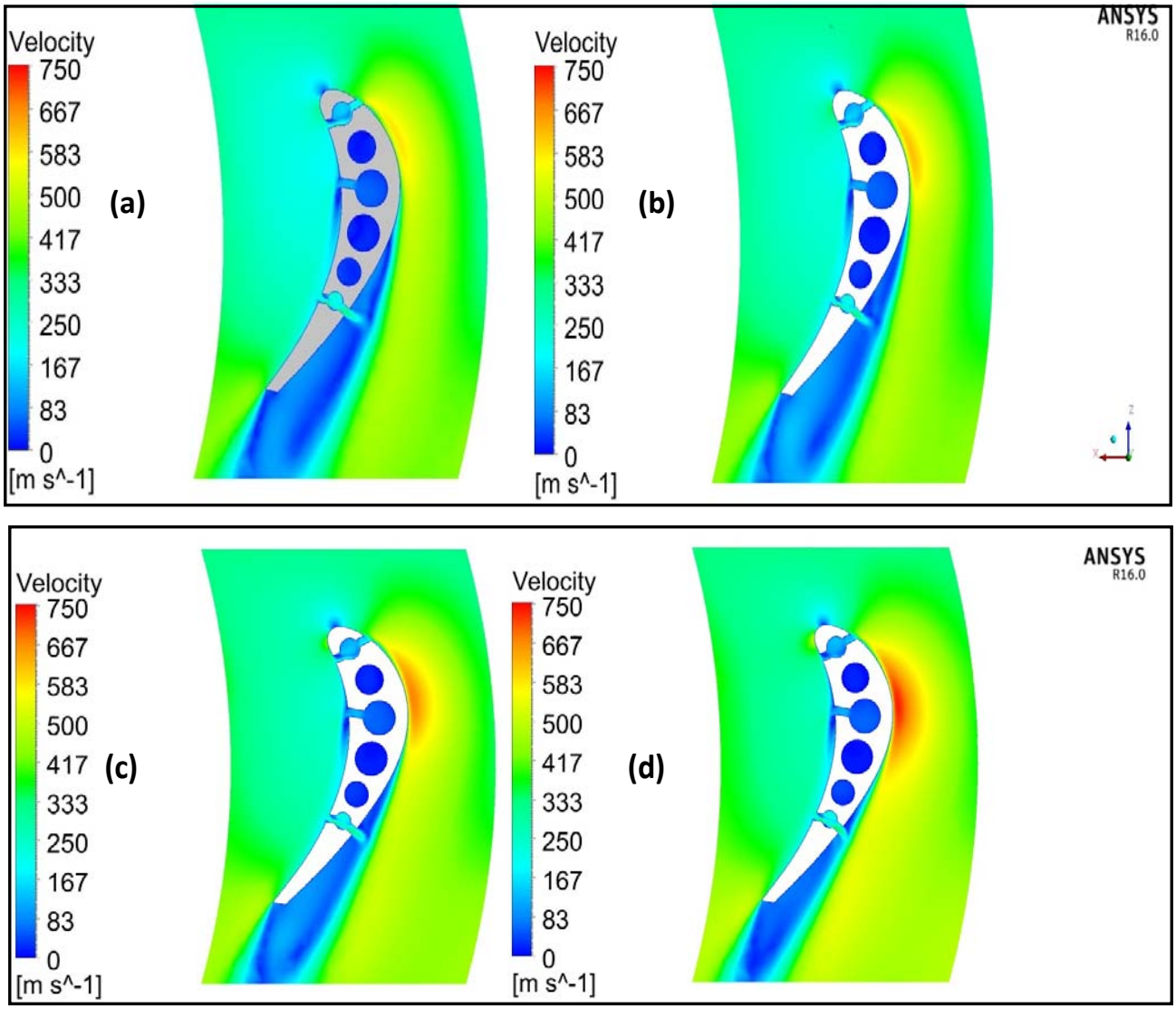

Figure 9: Velocity distribution at mid-span of the blade (a) TIT 900°C; (b) TIT 1000°C;(c) TIT 1100°C; and (d) TIT 1200°C

The Figure 9 range was fixed to compare the velocity of each turbine inlet temperature. The rise in temperature increases the gas flow velocity distribution. Then, it can be concluded that the temperature directly influences the velocity due the kinetic energy increase.

Table 6 show the maximum and minimum flow velocity (external and internal) for each gas turbine inlet temperature. Comparing the Figure 9 and Table 6, the maximum external flow velocity occurs on the suction side, and the minimum external flow velocity on the pressure side close to the film cooling. Concerning the internal air cooling, the minimum occurs at the cooling channel without the film cooling channels, and the maximum is reached at the boundary between the external and the internal fluids.

Table 5: Minimum and maximum velocity of the fluid

Turbine Inlet Temperature (°C)	Minimum velocity (m/s)	Maximum velocity (m/s)
900	External: 120 Internal: 24	External: 586 Internal: 282
1000	External: 168 Internal: 24	External: 617 Internal: 310
1100	External: 310 Internal: 24	External: 696 Internal: 354
1200	External: 343 Internal: 24	External: 749 Internal: 378

c) Thermodynamics - CFD

Every solution was converged between 800-1000 interactions with 45-55 hours of computation. The residuals of u-momentum, v-momentum and w-momentum were of order of 10^{-4} and the residual of the mass was the order of 10^{-5}.

The conjugate heat transfer obtained the blade temperature distribution. The temperature distribution of the substrate at the suction side and pressure side are shown in Figure10. This figure shows the temperature distribution - for each turbine inlet temperature. In addition, Figure 11 shows the temperature distribution for the blade at each span.

These figures show that the temperature distribution indicates that the suction side (SS) temperature is lower than the pressure side (PS) because the flow on the suction side was accelerated. As a result of the turbine inlet temperature profile, the gas temperature was higher at the blade mid-span, then the temperature was higher at the inlet blade mid-span. There is a lower temperature region at the root, where the coolant fluid is colder.

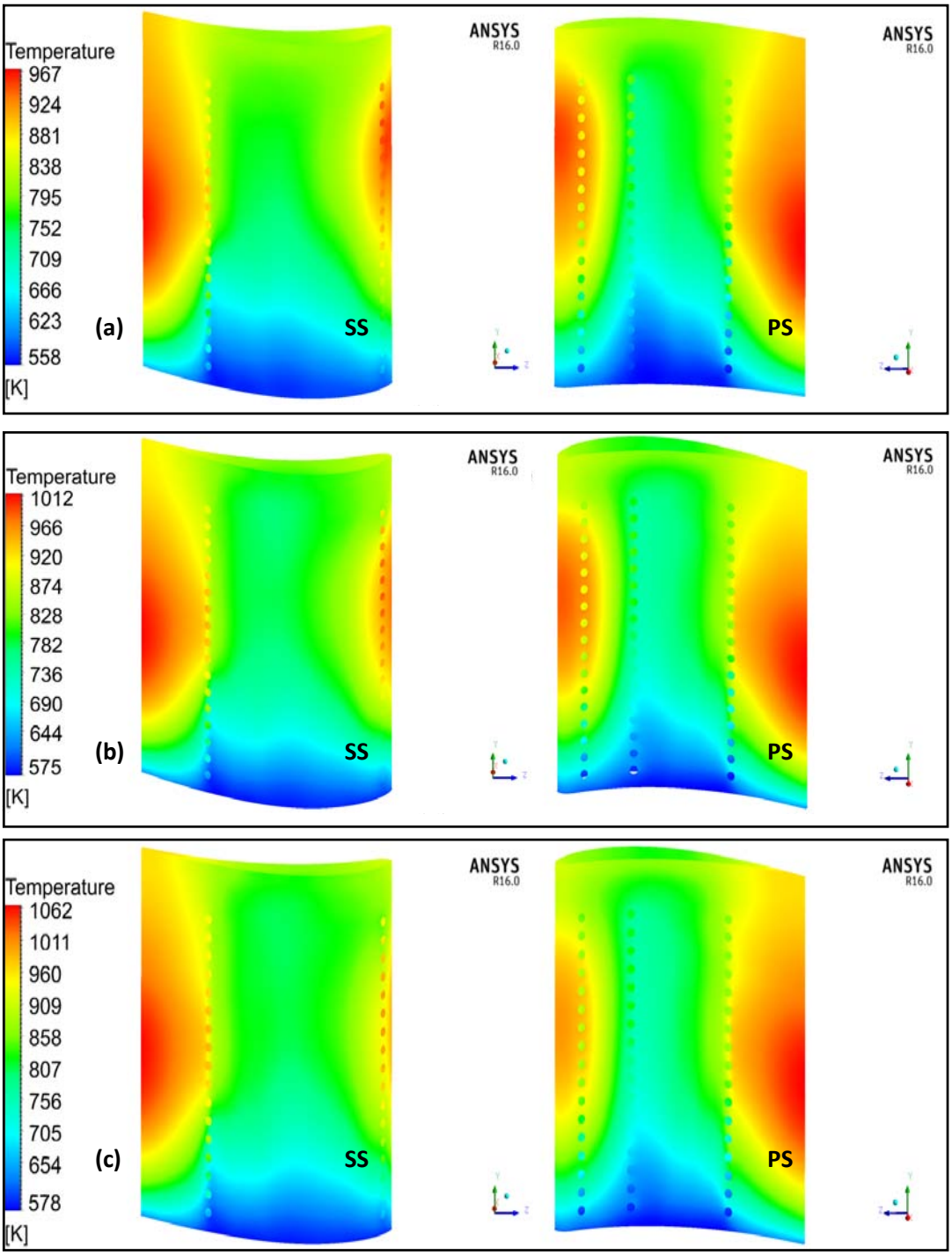

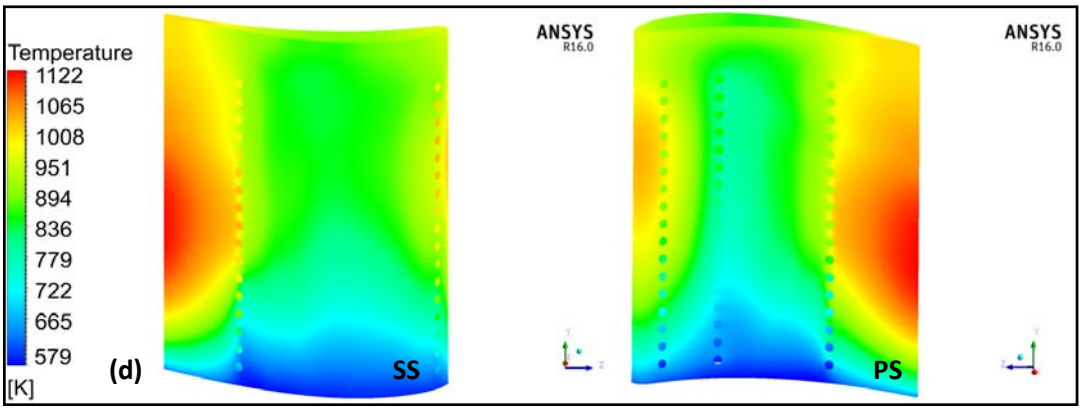

Figure 10: Temperature distribution on the substrate for (a) TIT 900°C; (b) TIT 1000°C;(c) TIT 1100°C; and (d) TIT 1200°C

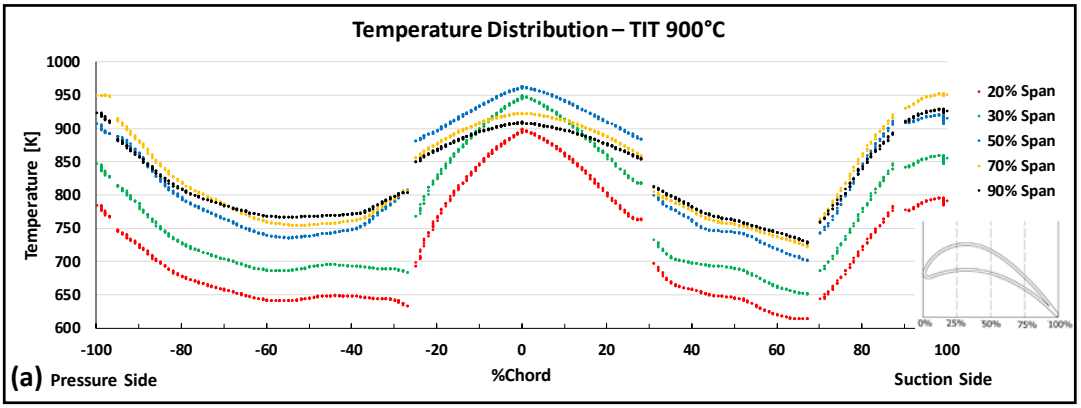

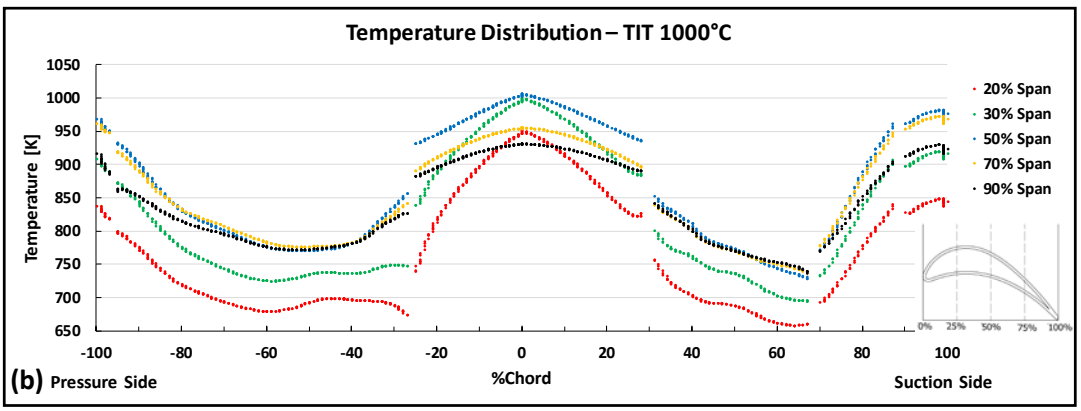

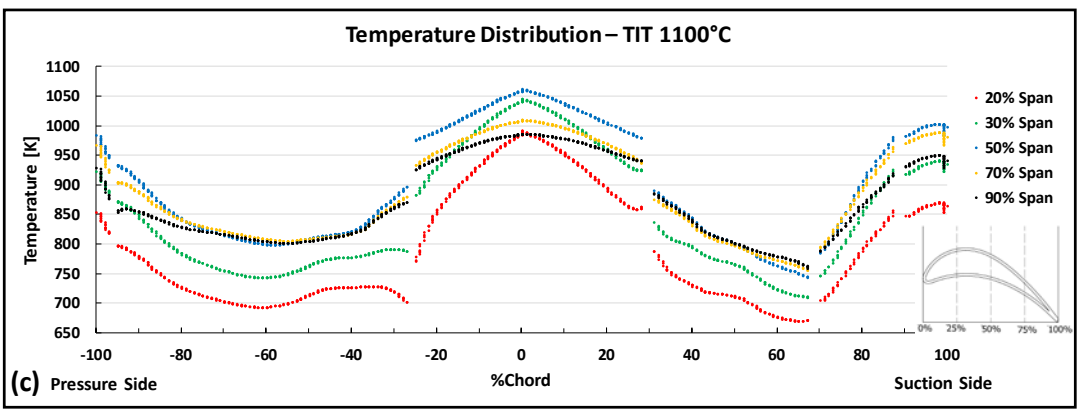

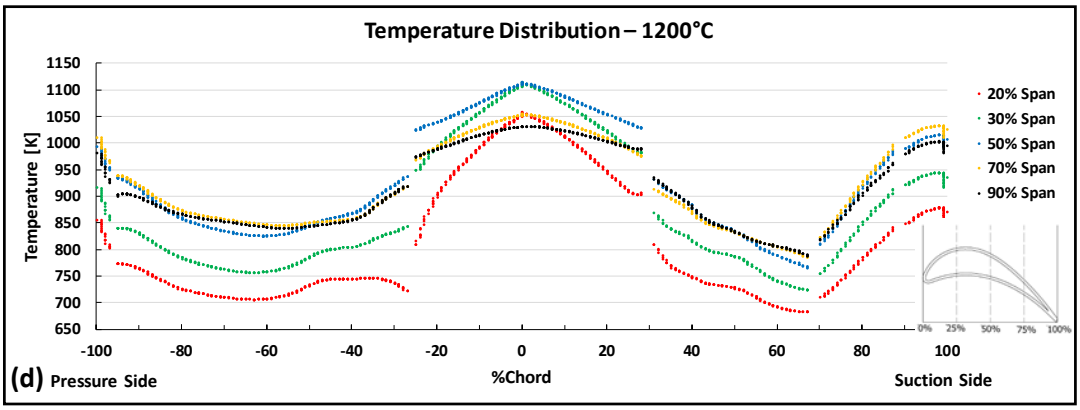

Figure 11: Temperature distribution for the blade at each span for (a) TIT 900°C; (b) TIT 1000°C;(c) TIT 1100°C; and (d) TIT 1200°C

The temperature distribution of the blade can be captured in Figures 10 and 11. From Figure 10, it can be seen clearly that hot spots exist at the leading edge and the trailing edge of the blade. Hot spot at the leading edge of the blade is observed at the mid-span (50% span) where the temperature of the gas flow is highest due to the turbine inlet temperature profile. The trailing edge hot spot is observed at 70% span of the blade where the cooling system is inefficient, and where the flow is converged due to tip leakage flow mentioned above. The gas flow vortexes affect the temperature distribution on the blade suction side and pressure side.

Then, the temperature increases gradually in a perpendicular direction to the blade rotation axis, the temperature drops sharply at blade center next to the root, indeed at this region the cooling has higher effectiveness. However, the cooling system is more effective at the TIT of 900°C. The thermal load on the suction side and on the pressure side declines gradually toward the mid span and rises gradually on the way to the trailing edge of the blade. In spite of that, the temperature reaches a maximum close to the leading edge at the mid-span while the minimum is next to the blade middle root. Table 5 shows the maximum temperature for each turbine inlet temperature and for each solid material.

Table 6: Maximum temperature for the solid materials

Turbine Inlet Temperature (°C)	Maximum temperature of AISI 316 (°C)	Maximum temperature of NiCrAlY (°C)	Maximum temperature of YSZ (°C)
900	694	737	739
1000	739	810	838
1100	789	856	919
1200	849	936	1036

The operating temperature of the AISI 316 austenitic stainless steel is 925°C for a constant temperature situation and 870°C for a variable temperature situation. The Table 5 and the experimental results of the furnace and the simulation, one can verify that the blade did not reach the temperature limit of operation for a constant temperature situation at the turbine inlet temperature of 900, 1000, 1100 and 1200°C. And the metallic substrate did not reach the temperature limit for a variable temperature situation. The thermal barrier coating and the cooling system reduces significantly the metal temperature.

d) Static Structural Analysis

Static structural analyses can be solved by the determination of the fluid-structural interaction and the turbine blade response due to mechanical loading provided by the fluid. In other words, the inlet parameters were

Obtained by fluid-solid interaction. It is used the pressure and temperature distribution given by the numerical solution through the dynamic computational method. The behavior of the fluid over the blade may be imported and this solution becomes the contour conditions of the structural analysis. The stresses distribution is shown in Figure 12.

From Figure 12, it can be seen that the highest values of von Mises stress occur close to the base of the blade, in the region of the coating, with values of 333.92 MPa, 333.58 MPa, 334.32 MPa and 327.33 MPa, at temperatures of 900°C, 1000°C, 1100°C and 1200°C, respectively. The maximum deformation is located at the blade top and the deformation has the tendency to elongate and twist the blade. Therefore, this region can

be more susceptible to thermo-mechanical fatigue and coating cracking, causing coating failure.

IV. Conclusions

Simulation and experiment were conducted in order to predict the turbine blade temperature distribution. The aim was to verify the stainless steel temperature and behavior under cooling and the thermal barrier coating effect on the thermal insulation.

From the experimental results of the furnace and the simulation, it can be concluded that the blade did not reach the temperature limit of operation for a constant and variable temperature situation at every turbine inlet temperature.

The effect of the thermal barrier coating, with the cooling system, is to decrease the temperature of the steel by approximately 160°C for each turbine inlet temperature. The cooling effect was very high at the regions close to blade center and close to the blade root.

The structural analysis shows that the blade got a tendency to develop a coating crack in the region close to the base. The stresses at the blade develop a deformation that elongate and twist the blade.

The stainless steel blade withstands the temperature distribution and the stress load applied. In conclusion, the austenitic stainless steel can be used as a turbine blade.

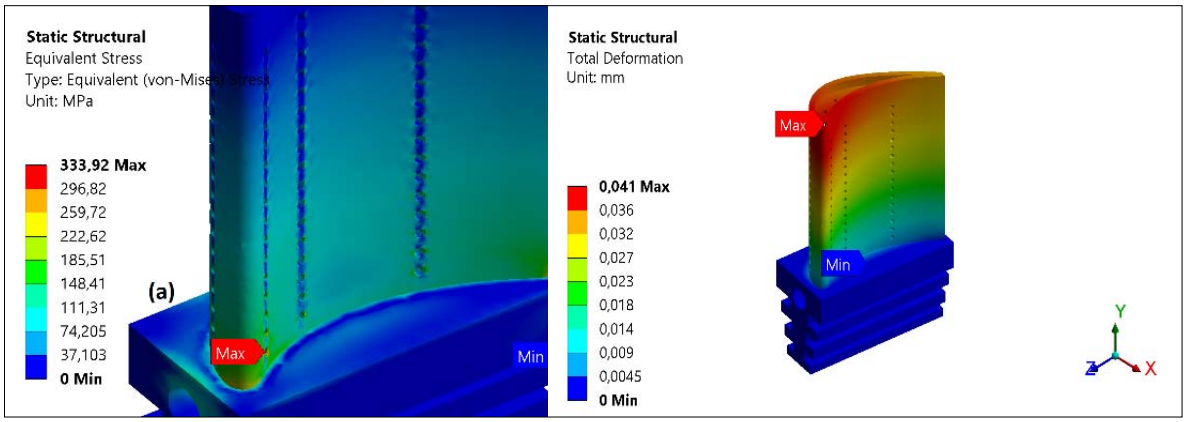

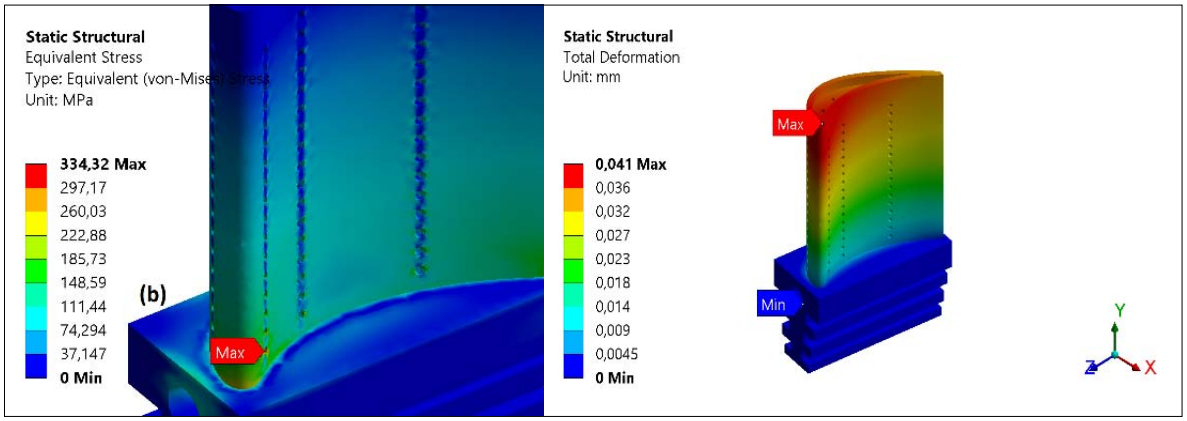

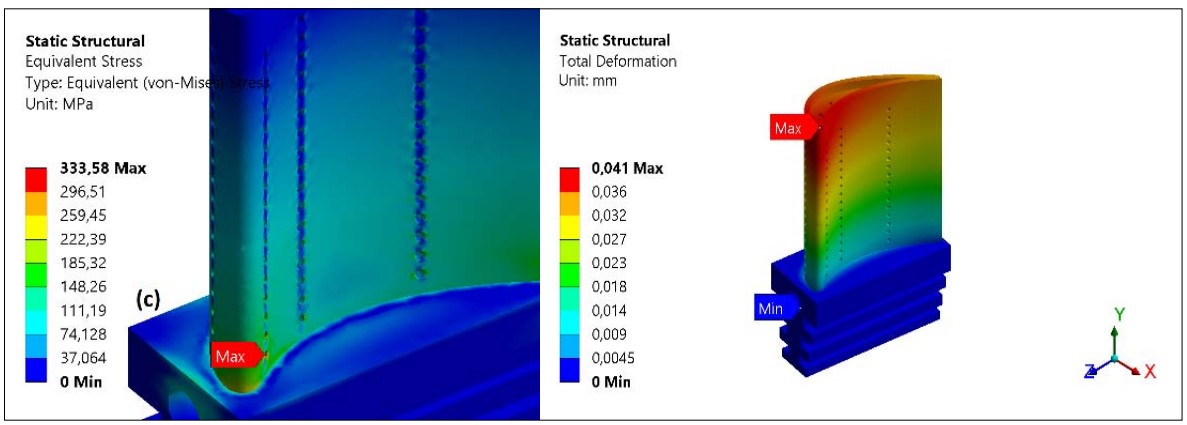

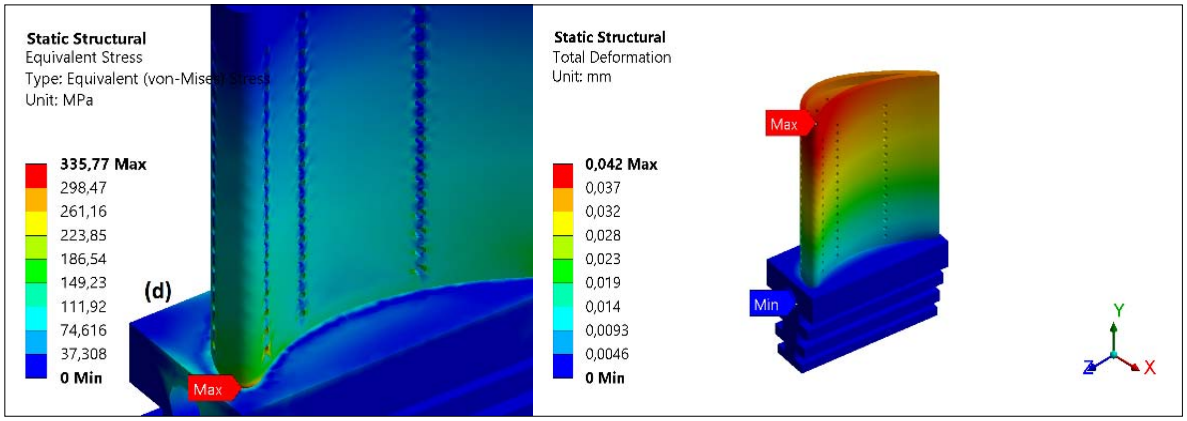

Figure 12: Stress and deformation distribution on the blade at TIT of (a) 900°C; (b) 1000°C; (c) 1100°C; and (d) 1200°C

Acknowledgments

The authors would like to acknowledge the Federal University of Ouro Preto, REDEMAT (Master and Doctorate Program at UFOP-UEMG), and Gorceix Foundation.

Nomenclature

ρ	Specific Mass (kg/m³)
t	Time (s)
U,V,W	Velocity vectors in the x-direction, y-direction, z-direction(m/s)
p	Stagnation pressure(Pa)
τ	Shear stress (Pa)
S_M	Momentum source (N.m)
h	Stagnation enthalpy (J/kg)
λ	Thermal conductivity (W/m.K)
S_E	Energy source (J)
T	Temperature (K)
c	Specific heat at constant pressure (J/mol.K)
α	Thermal expansion coefficient (1/°C)
σ	Normal stress(Pa)
f	Force(N)
E	Elastic modulus(Pa)
υ	Poisson coefficient (-)
ε	Normal strain (-)
γ	Shear strain (-)
Subscripts	
tot	Total
s	Solid
i	xversor
j	yversor
k	zversor

Abreviations

TBC	Thermal barrier coating
TC	Top coat
TGO	Thermally grown oxide
BC	Bond coat
CHT	Conjugate heat transfer
CFD	Computational fluid dynamics
YSZ	Yttria-stabilized zirconia
GT	Gas turbine
SST	Shear stress transport
LPG	Liquefied petroleum gas
TIT	Turbine inlet temperature
SS	Suction Side
PS	Pressure Side

References Références Referencias

1. Ogbonnaya Agwu, Chigozie Eleghasim. Mechanical Drive gas Turbine Selection for Service in two Natural gas Pipelines In Nigeria. Case Studies in Thermal Engineering, V. 10: 19-27, 2017 (Http://Dx.Doi.Org/10.1016/J.Csite.2017.02.003).
2. Osamu Kurata, Norihiko Iki, Takayuki Matsunuma, Takahiro Inoue, Taku Tsujimura, Hirohide Furutani, Hideaki Kobayashi, Akihiro Hayakawa. Performances and Emission Characteristics of Nh_3–Air and Nh_3ch_4–Air Combustion Gas-Turbine Power Generation. Proceedings of the Combustion Institute, V. 36(3): 3351-3359, 2017. (Http://Dx.Doi.Org/10.1016/J.Proci.2016.07.088).
3. Jorge Sousa, Guillermo Paniagua, Elena Collado Morata.Thermodynamic Analysis of a Gas Turbine Engine With a Rotating Detonation Combustor. Applied Energy, V. 195: 247256 2017. (Http://Dx.Doi.Org/10.1016/J.Apenergy.2017.03.04).
4. Canan U. Hardwicke, Yuk-Chiu Lau. Advances in Thermal Spray Coatings for Gas Turbines and Energy Generation: a Review. Journal of Thermal Spray Technology, V.22: 564–576, 2013. (Doi:10.1007/S11666-013-9904-0).
5. Abdul Ghafoor Memon, Khanji Harijan, Mohammad Aslam Uqaili, Rizwan Ahmed Memon. Thermo-Environmental and Economic Analysis of Simple and Regenerative Gas Turbine Cycles With Regression Modeling and Optimization. Energy Conversion and Management, V. 76: 852-864, 2013. (Http://Dx.Doi.Org/10.1016/J.Enconman.2013.07.076).
6. G.W Goward. Progress in Coatings For Gas Turbine Airfoils. Surface and Coatings Technology, V. 108–109: 73-79, 1998. (Http://Dx.Doi.Org/10.1016/S0257-8972(98)00667-7).
7. M. Martena, D. Botto, P. Fino, S. Sabbadini, M.M. Gola, C. Badini. Modelling of Tbc System Failure: Stress Distribution as a Function of Tgo Thickness and Thermal Expansion Mismatch. Engineering Failure Analysis, V. 13(3): 409-426, 2006. (Https://Doi.Org/10.1016/J.Engfailanal.2004.12.027.)
8. Sushila Rani, Atul K. Agrawal, Vikas Rastogi.Failure Analysis of a first Stage In738 gas Turbine Blade tip Cracking in a thermal power Plant. case studies in Engineering Failure Analysis, V. 8:1-10,320 10. (Http://Dx.Doi.Org/10.1016/J.Csefa.2016.11.0020.
9. R. Sivakumar, B. L. Mordike. High Temperature Coatings for Gas Turbine Blades: a Review, Surface and Coatings Technology, V. 37(2): 139-160, 1989. (Http://Dx.Doi.Org/10.1016/0257-8972(89)90099-6).
10. W. Zhu, M. Cai, L. Yang, J.W. Guo, Y.C. Zhou, C. Lu. The Effect of Morphology of Thermally Grown Oxide on the Stress Field in a Turbine Blade with Thermal Barrier Coatings. Surface and Coatings Technology, V. 276: 160-167, 2015. (Http://Dx.Doi.Org/10.1016/J.Surfcoat.2015.06.061).
11. Tafti Dk, He L, Nagendra K. Large Eddy Simulation for Predicting Turbulent Heat Transfer in Gas Turbines. Philos Trans a Math Phys Eng Sci. 2014 372(2022):20130322.(Doi:10.1098/Rsta.2013.0322).
12. Vijay K. Garg. Heat Transfer Research on Gas Turbine Airfoils at Nasa Grc, International Journal of Heat and Fluid Flow, V. 23(2): 109-136, 2002. (Http://Dx.Doi.Org/10.1016/S0142-727x(01)00144-8)
13. T. Sadowski, P. Golewski. Multidisciplinary Analysis of the Operational Temperature Increase of Turbine Blades in Combustion Engines by Application of the Ceramic Thermal Barrier Coatings (Tbc). Computational Materials Science, V. 50(4): 1326 – 1335,2011. (Http://Dx.Doi.Org/10.1016/J.Commatsci.2010.05.032).
14. Majid Rezazadeh Reyhani, Mohammad Alizadeh, Alireza Fathi, Hiwa Khaledi. Turbine Blade Temperature Calculation and Life Estimation - a Sensitivity Analysis. Propulsion and Power Research, V. 2(2): 148-161, 2013. (Http://Dx.Doi.Org/10.1016/J.Jppr.2013.04.004).
15. Zdzislaw Mazur, Alejandro Hernández-Rossette, Rafael García-Illescas, Alberto Luna-Ramírez,

Analysis of Conjugate Heat Transfer of a Gas Turbine first Stage nozzle. applied Thermal Engineering, V. 26(16): 1796-1806, 2006. (Http://Dx.Doi.Org/10.1016/J.Applthermaleng.2006.01.025).

16. D. Bohn, B. Bonh off, H. Schonenborn. Combined Aerodynamic And Thermal Analysis of a Turbine Nozzle Guide Vane. Proceedings of the 1995 Yokohama International Gas Turbine Congress, October 22 - 27, 1995.
17. Dieter E. Bohn, Volker J. Becker, Agnes U. Rungen. Experimental and Numerical Conjugate Flow and Heat Transfer Investigation of a Shower Head Cooled Turbine Guide Vane. Asme 1997 International Gas Turbine and Aeroengine Congress and Exhibition. Volume 3: Heat Transfer; Electric Power; Industrial and Cogeneration. Orlando, Florida, Usa, June 2–5, 1997 (Isbn: 978-0-7918-7870-5)
18. Dieter E. Bohn, Volker J. Becker, Karsten a. Kusterer. 3-D Conjugate Flow and Heat Transfer Calculations of a Film Cooled Turbine Vane at Different Operation Conditions. Asme 1997 International Gas Turbine And Aeroengine Congress And Exhibition
19. F. Jamarani, M. Korotkin, R. V. Lang, M. F. Ouellette, K. L. Yan, R. W. Bertram, V. R. Parameswaran. Compositionally Graded Thermal Barrier Coatings For High Temperature Aero Gas Turbine Components, Surface and Coatings Technology, Volume 54, 1992, Pages 58-63, Issn 0257-8972, Http://Dx.Doi.Org/10.1016/S0257-8972(09)90028-7.
20. P. Scardi, M. Leoni, F. Cernuschi; A. Figari. Microstructure and Heat Transfer Phenomena in Ceramic Thermal Barrier Coatings. Journal of the American Ceramic Society, V. 84: 827–835. 2001. (Doi:10.1111/J.1151-2916.2001.Tb00748.X)
21. Teleginski, D. C. Chagas, A. C. C. Oliveira, J. C. G. Santos, J. F. Azevedo, R. Riva, G. Vasconcelos. Yb: Fiber Laser Surface Texturing of Stainless Steel Substrate, with Mcraly Deposition and Co_2 Laser Treatment. Surface and Coatings Technology, V. 260: 251-259, 2014. (Http://Dx.Doi.Org/10.1016/J.Surfcoat.2014.06.076).
22. A. S. Osyka, A. I. Rybnikov, S. A. Leontiev, N. V. Nikitin, I. S. Malashenko. Experience With Metal/Ceramic Coating In Stationary Gas Turbines. Surface and Coatings Technology, V. 76: 86-94, 1995. (Http://Dx.Doi.Org/10.1016/0257-8972(95)02541-3).
23. D. R. Clarke, M. Oechsner, N. P. Padture. Thermal-Barrier Coatings for More Efficient Gas-Turbine Engines. Mrs Bulletin, V. 37: 891-898, 2012. (Https://Doi.Org/10.1557/Mrs.2012.232).
24. J. H. Liu, Y. B. Liu, X. He, L. Liu. Study on Tbcs Insulation Characteristics of A Turbine Blade Under Serving Conditions. Case Studies in Thermal Engineering, V. 8: 250-259, 2016. (Http://Dx.Doi.Org/10.1016/J.Csite.2016.08.004).
25. Sunwoo Hwang, Changmin Son, Doyoung Seo, Dong-Ho Rhee, Bongjun Cha. Comparative Study on Steady and Unsteady Conjugate Heat Transfer Analysis of a High Pressure Turbine Blade. Applied Thermal Engineering, V. 99: 765-775, 2016. (Https://Doi.Org/10.1016/J.Applthermaleng.2015.12.139).
26. Ansys. Ansys Cfx - Solver Theory Guide. Canonsburg: Ansys, Inc., 2013.
27. W. D. Callister; D. G. Rethwisch. Materials Science and Engineering: An Introduction. 8ª. Ed. usa: Wiley, 2010.
28. J. W. Adams, R. Ruh, K. S. Mazdiyasni. Young's Modulus, Flexural Strength, and Fracture Of Yttria-Stabilized Zirconia Versus Temperature. Journal Of The American Ceramic Society, 80: 903–908, 1997. (Doi:10.1111/J.1151-2916.1997.Tb02920).
29. L. S. Cook, A. Wolfenden, W. J. Brindley. Temperature Dependence of Dynamic Young's Modulus and Internal Friction in Lpps Nicraly. Journal of Materials Science, V. 29(19): 5104–5108,1994. (Doi:10.1007/Bf01151103).
30. H. Cohen, G. F. C. Rogers, H. I. H. Saravanamuttoo. Gas Turbine Theory. 4ª. Ed. Harlow: Longman Group, 1996.